Inorganic Chemistry

including bioinorganic chemistry

December 16, 2013
Volume 52, Number 24
pubs.acs.org/IC

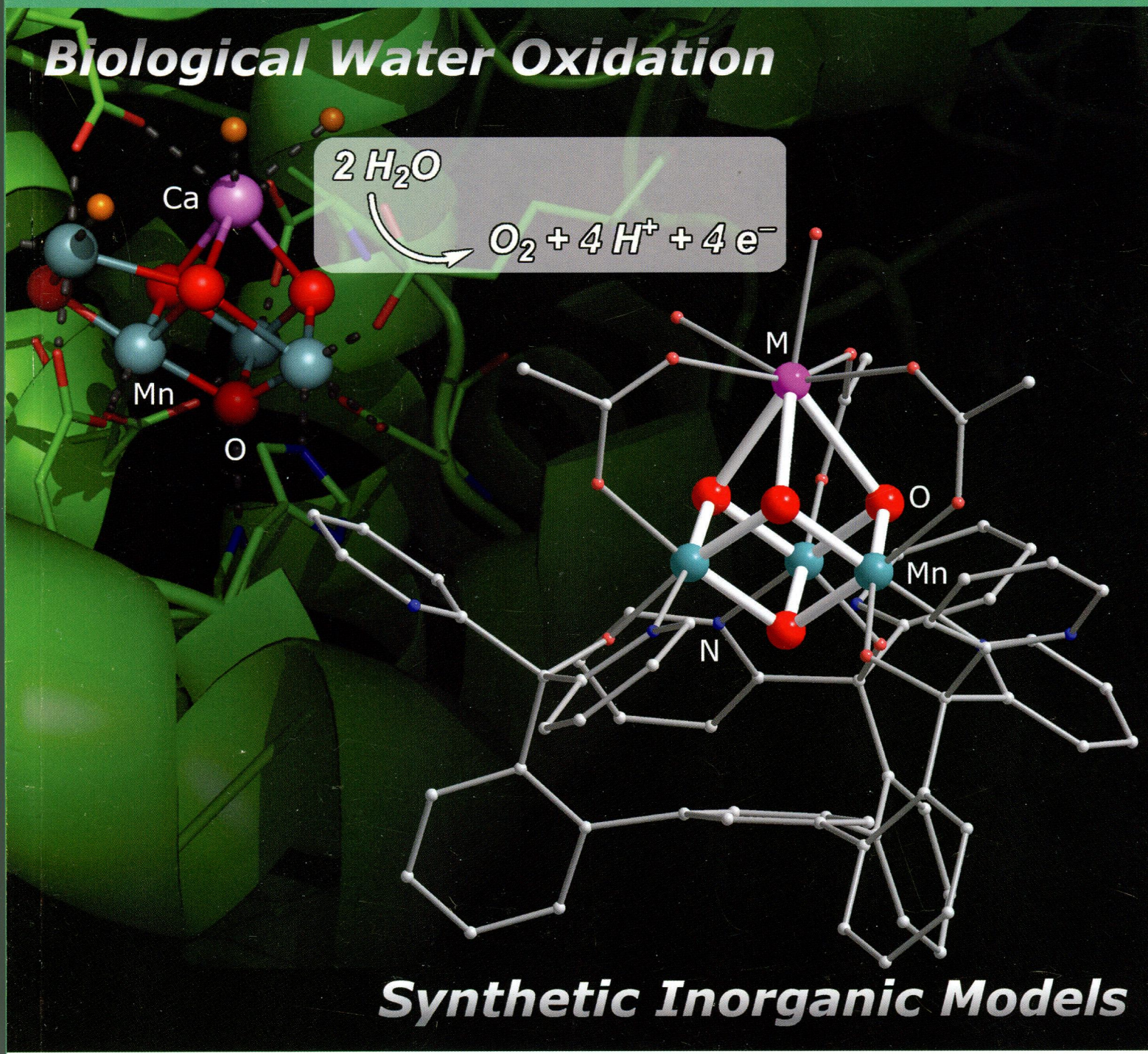

ACS Publications
MOST TRUSTED. MOST CITED. MOST READ.
www.acs.org

Inorganic Chemistry

DECEMBER 16, 2013
VOLUME 52 ISSUE 24

INOCAJ 52(24) 13803–14450 (2013)
ISSN 0020-1669
Registered in the U.S. Patent and Trademark Office

ON THE COVER: The oxygen-evolving complex of photosystem II is a calcium/manganese cluster that performs the photosynthetic oxidation of water to dioxygen (top left). Structurally related synthetic inorganic models are employed to advance the understanding of the reactivity and redox properties of this important biological cluster (bottom right). See E. Y. Tsui, J. S. Kanady, and T. Agapie, p 13833.

Communications

13809 dx.doi.org/10.1021/ic4022678

Substituent-Dependent Spin-Density Distribution and Coexistence of Fe 3d and π Spins on Ferrocene–Tetrathiafulvalene Hybrids

Tetsuro Kusamoto,* Hiroshi Nishihara, and Reizo Kato

Ferrocene (Fc) and tetrathiafulvalene (TTF) moieties were incorporated into novel hybrid molecules of structure $FcS_4TTF(R)_2$ (R = CF_3 and SMe). $[FcS_4TTF(R)_2]^{\bullet+}$ exhibited R-dependent spin-density distribution, and $[FcS_4TTF(CF_3)_2]^{\bullet 2+}$ showed the coexistence of Fc-centered Fe 3d and TTF-centered π spins. The solid-state molecular structures in different oxidation states reflect their characteristic spin states.

< Solid-state molecular structures >

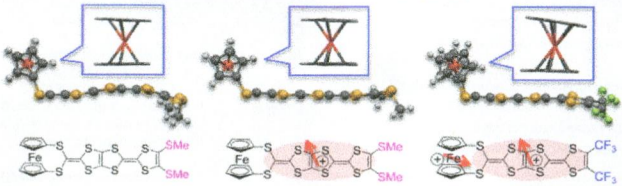

13812 dx.doi.org/10.1021/ic402277x

Negative Differential Resistance in MX- and MMX-Type Iodide-Bridged Platinum Complexes

Hiroaki Iguchi,* Shinya Takaishi, Deli Jiang, Jimin Xie, Masahiro Yamashita,* Atsuko Uchida, and Hitoshi Kawaji

Negative differential resistance (NDR) was discovered in semiconductive MX- and MMX-type iodide-bridged platinum complexes for the first time. Joule heat affects the low resistance of the complexes observed under the large current, but it could not perfectly explain the NDR. The intrinsic charge-ordering states are considered to contribute to the NDR of these compounds.

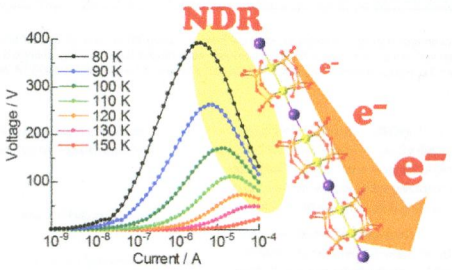

13815 dx.doi.org/10.1021/ic402428m

In Situ Construction of a Coordination Zirconocene Tetrahedron

Guoliang Liu, Zhanfeng Ju, Daqiang Yuan,* and Maochun Hong

The design and synthesis of new Platonic and Archimedean polyhedra through coordination-driven self-assembly have consistently become an active field of supramolecular chemistry and crystal engineering. The current study describes the first in situ synthesis of a new family of cationic coordination tetrahedra with isostructural supramolecular structure based on trinuclear zirconocene nodes and dicarboxylate or tricarboxylate anions.

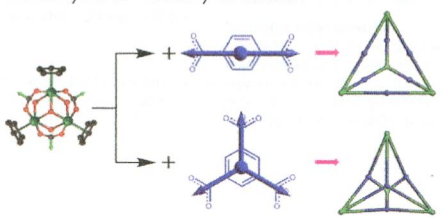

13818 S dx.doi.org/10.1021/ic402435z

Crystalline Fibers of Metal–Peptide Double Ladders

Dani Peri, Jim Ciston, Felipe Gándara, Yingbo Zhao, and Omar M. Yaghi*

Despite remarkable progress in the field of MOFs, structures based on long-flexible organic linkers are scarce and the majority of such materials rely on rigid linkers. In this work, crystals of a new metal–organic double ladder (MODL) are obtained by linking a pentapeptide (NH_2-Glu-$p$$CO_2$Phe-$p$$CO_2$Phe-Ala-Gly-OH) with cadmium acetate to produce a Cd(2-pyrrolidone-$p$$CO_2$Phe-$p$$CO_2$Phe-Ala-Gly)$(H_2O)_3$ framework. SEM and TEM analyses show the fibrous nature of the crystals and show that the infinite cadmium oxide rod secondary building units (SBUs) are aligned with the longitudinal axis of the nanofibers.

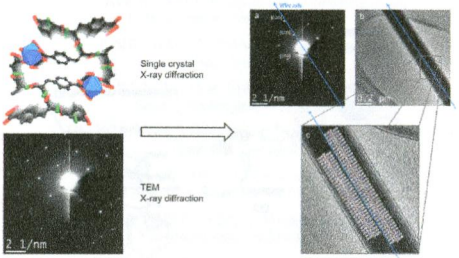

13821 S dx.doi.org/10.1021/ic402556g

Cage Shrinkage of Fullerene via a C_2 Loss: from IPR $C_{90}(28)Cl_{24}$ to Nonclassical, Heptagon-Containing $C_{88}Cl_{22/24}$

Ilya N. Ioffe,* Olga N. Mazaleva, Lev N. Sidorov, Shangfeng Yang,* Tao Wei, Erhard Kemnitz, and Sergey I. Troyanov*

A new case of chlorination-promoted fullerene cage shrinkage is reported. Chlorination of C_{90} (isolated pentagon rule isomer no. 28) with VCl_4 afforded $C_{88}Cl_{22}$ with a nonclassical carbon cage (NCC) containing 1 heptagon and 13 pentagons including 2 fused pairs flanking the heptagon (see diagram). The pathway of C_2 abstraction from the C_{90} cage is suggested on the basis of density functional theory calculations.

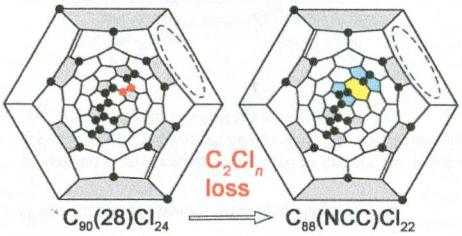

13824 S dx.doi.org/10.1021/ic402579v

$AgCu_3V_4O_{12}$: a Novel Perovskite Containing Mixed-Valence Silver ions

Yasuhide Akizuki, Ikuya Yamada,* Koji Fujita,* Hirofumi Akamatsu, Tetsuo Irifune, and Katsuhisa Tanaka

A novel A-site-ordered perovskite, $AgCu_3V_4O_{12}$, has been synthesized at a high temperature of 1373 K and a high pressure of 15 GPa. In this compound, Ag ions occupy a 12-coordinated site to form regular icosahedra and are present in the mixed-valence state. $AgCu_3V_4O_{12}$ exhibits metallic behavior, and it is expected from the electronic structure calculations that the Ag 4d electrons as well as Cu and V 3d electrons are delocalized to cause metallic conduction.

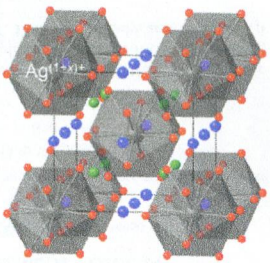

13827 (S) dx.doi.org/10.1021/ic402611m

Peculiar Features in the Crystal Structure of the Adduct Formed between *cis*-$PtI_2(NH_3)_2$ and Hen Egg White Lysozyme

Luigi Messori,* Tiziano Marzo, Chiara Gabbiani, Amparo A. Valdes, Adoracion G. Quiroga, and Antonello Merlino*

The reactivity of *cis*-$PtI_2(NH_3)_2$, the iodo analogue of cisplatin, with HEWL was investigated by X-ray crystallography and electrospray ionization mass spectrometry. In the resulting adduct, the Pt^{II} center selectively coordinates to the imidazole of His15 with the release of one ammonia ligand. Interestingly, both iodide ligands remain bound to platinum. Two equivalent modes of Pt^{II} binding are possible that differ only in the location of I atoms with respect to ND1 of His15. The structure of the adduct was compared with that of HEWL–cisplatin.

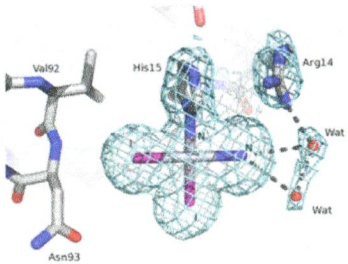

13830 (S) dx.doi.org/10.1021/ic402763z

Fluorescent Organic Nanoparticles of Biginelli-Based Molecules: Recognition of Hg^{2+} and Cl^- in an Aqueous Medium

Ajnesh Singh, Tilak Raj, Thammarat Aree, and Narinder Singh*

Fluorescent organic nanoparticles of three new Biginelli-based molecules have been developed as chemosensors for chromogenic and fluorogenic detection of Hg^{2+} and chromogenic detection of Cl^- ions in an aqueous medium. The probes can detect Hg^{2+} and Cl^- ions up to nanomolar and micromolar ranges in an aqueous medium, respectively.

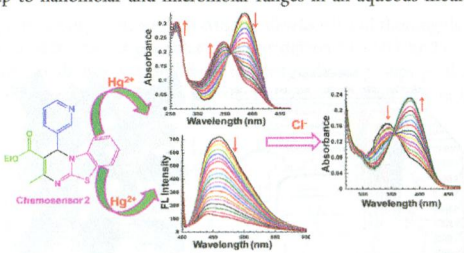

Award Paper

13833 dx.doi.org/10.1021/ic402236f

Synthetic Cluster Models of Biological and Heterogeneous Manganese Catalysts for O_2 Evolution

Emily Y. Tsui, Jacob S. Kanady, and Theodor Agapie*

Understanding the mechanism of water oxidation to O_2 is important for the rational design of practical catalysts for artificial photosynthesis. This Award Article reviews recent developments in the synthesis of heterometallic structural models of the oxygen-evolving complex of photosystem II. Access to discrete models has allowed insightful structure–property studies. Implications for the function of the biological and heterogeneous catalysts are discussed

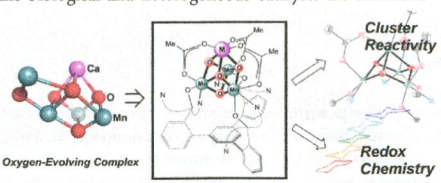

Articles

13849 S dx.doi.org/10.1021/ic401036e

Heptanuclear Antiferromagnetic Fe(III)–D-(-)-Quinato Assemblies with an $S = 3/2$ Ground State—pH-Specific Synthetic Chemistry, Spectroscopic, Structural, and Magnetic Susceptibility Studies

M. Menelaou, E. Vournari, V. Psycharis, C. P. Raptopoulou, A. Terzis, V. Tangoulis, Y. Sanakis, C. Mateescu, and A. Salifoglou*

pH-specific stoichiometric reactions of basic iron-acetate and Mohr's salt with D-(-)-quinic acid led to the heptanuclear compounds $[Fe_7O_3(OH)_3(C_7H_{10}O_6)_6]\cdot 20.5H_2O$ (**1**) and $(NH_4)[Fe_7(OH)_6(C_7H_{10}O_6)_6]\cdot(SO_4)_2\cdot 18H_2O$ (**2**), exhibiting an overall antiferromagnetic behavior with a ground state $S = 3/2$. These compounds were characterized by analytical, spectroscopic, electrochemical, thermal, magnetic, and structural techniques. Their collective physicochemical profiles reflect (a) diverse pH-specific reactivity in aqueous Fe(II,III)–quinato binary systems and (b) factors–conditions influencing multinuclear Fe(III)–hydroxycarboxylato assemblies of defined lattice architecture-dimensionality and magnetostructural properties.

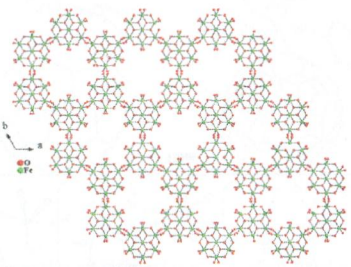

13861 S dx.doi.org/10.1021/ic401144k

Ion-Exchange Synthesis, Crystal Structure, and Physical Properties of Hydrogen Titanium Oxide $H_2Ti_3O_7$

Kunimitsu Kataoka,* Norihito Kijima, and Junji Akimoto*

$H_2Ti_3O_7$ prepared via Na^+/H^+ ion exchange in acidic solution at 333 K. The crysta structure was refined by neutron diffraction.

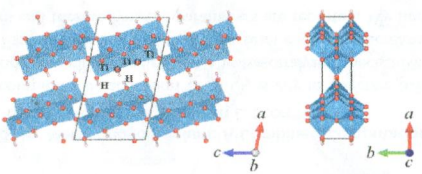

Crystal structure of $H_2Ti_3O_7$

13865 S dx.doi.org/10.1021/ic401486y

Synthesis and Characterization of Terpyridine-Supported Boron Cations: Evidence for Pentacoordination at Boron

Gregory P. McGovern, Di Zhu, Adelia J. A. Aquino, Dragoslav Vidović,* and Michael Findlater*

A rare hypervalent interaction is found in a formally dicationic boron complex; the novelty of the structure arises from the absence of a rigidly prearranged pocket to force pentacoordination.

To bond or not to bond...

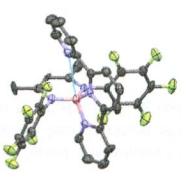

that is the coordination number

13869 Ⓢ dx.doi.org/10.1021/ic4025316

New Layered-Type Quaternary Chalcogenides, Tl_2PbMQ_4 (M = Zr, Hf; Q = S, Se): Structure, Electronic Structure, and Electrical Transport Properties

Cheriyedath Raj Sankar, Abdeljalil Assoud, and Holger Kleinke*

The new chalcogenides Tl_2PbMQ_4 (M = Zr, Hf; Q = S, Se) adopt a unique layered structure composed of alternating metal and chalcogen layers. The metal slabs alternate between Tl layers and mixed Pb/Zr layers. All metal atoms are located in differently distorted Q_6 octahedra, with the TlQ_6 polyhedra being the least regular ones. These chalcogenides are dark, narrow gap semiconductors, in agreement with the charge-balanced formula $(Tl^+)_2Pb^{2+}M^{4+}(Q^{2-})_4$.

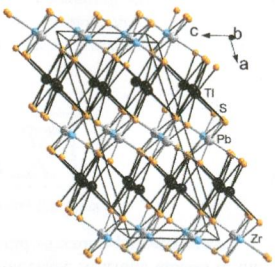

13875 Ⓢ dx.doi.org/10.1021/ic401262w

$Na_2CaSn_2Ge_3O_{12}$: A Novel Host Lattice for Sm^{3+}-Doped Long-Persistent Phosphorescence Materials Emitting Reddish Orange Light

Jiao Xu, Zhenghua Ju, Xiuping Gao, Yanqing An, Xiaoliang Tang, and Weisheng Liu*

A novel type host lattice $Na_2CaSn_2Ge_3O_{12}$ was first utilized for synthesizing reddish orange long-persistent phosphorescence materials. The optics properties of $Na_2CaSn_2Ge_3O_{12}$:Sm^{3+} were discussed.

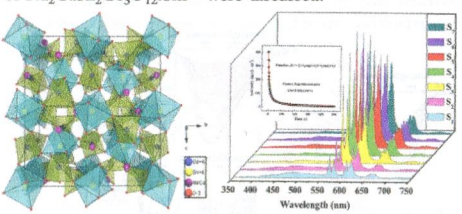

13882 Ⓢ dx.doi.org/10.1021/ic401296f

Metal–Ligand Synergistic Effects in the Complex Ni(η^2-TEMPO)$_2$: Synthesis, Structures, and Reactivity

Derek Isrow, Nathan J. DeYonker, Anjaneyulu Koppaka, Perry J. Pellechia, Charles Edwin Webster,* and Burjor Captain*

The bifunctional cooperativity between the hemilabile nature of the TEMPO ligand to interconvert between η^2 and η^1-binding modes, and the nickel center in the complex Ni(η^2-TEMPO)$_2$ **1** facilitates its reactivity with organic substrates at 25 °C. Compound **1** reacts with terminal alkynes to yield the respective acetylide products in a unique manner as seen in **8** and **9**, with the N atom on the TEMPO ligand acting as a base to abstract the H atom off the alkyne moiety.

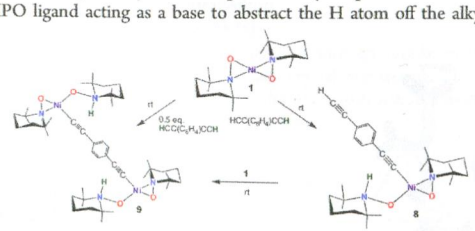

13894 S dx.doi.org/10.1021/ic401337q

Self-Assembled Tetra- and Pentanuclear Nickel(II) Aggregates From Phenoxido-Based Ligand -Bound {Ni_2} Fragments: Carboxylate Bridge Controlled Structures

Aloke Kumar Ghosh, Michael Shatruk, Valerio Bertolasi, Kausikisankar Pramanik, and Debashis Ray*

Carboxylato-bridge-dependent supramolecular [Ni_4] and [Ni_5] aggregate formation within same ligand environment have been examined through varying course of coordination cluster assembly based on [Ni_2] fragments. Incorporation of these bridges gave magnetically interesting compounds having $S = 3$ and 4 ground states also linked to crystal packing and separation between the clusters in solid state crystal packing.

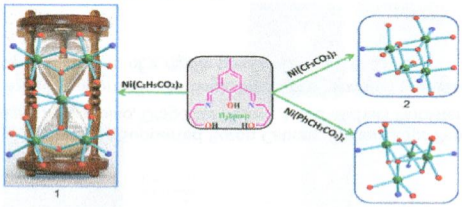

13904 S dx.doi.org/10.1021/ic401343m

Water-Catalyzed Activation of H_2O_2 by Methyltrioxorhenium: A Combined Computational−Experimental Study

Taeho Hwang, Bryan R. Goldsmith, Baron Peters,* and Susannah L. Scott*

The formation of peroxorhenium complexes by activation of H_2O_2 is key in selective oxidations catalyzed by CH_3ReO_3. Computed rate constants that include tunneling predict that a water-catalyzed mechanism is at least 7 orders of magnitude faster than direct ligand exchange. Experiments confirm that the rate of each step increases rapidly with water concentration, and consistent activation parameters and thermodynamic parameters are reported. We find reasonable agreement in this first direct comparison of computed and observed rate constants.

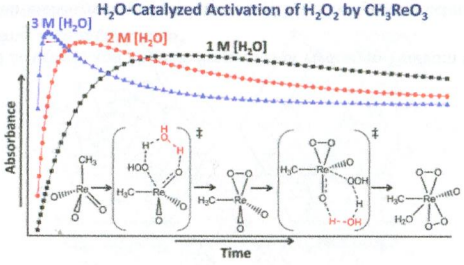

13918 S dx.doi.org/10.1021/ic402364p

Formation Pathway of Roussin's Red Ester (RRE) via the Reaction of a $\{Fe(NO)_2\}^{10}$ Dinitrosyliron Complex (DNIC) and Thiol: Facile Synthetic Route for Synthesizing Cysteine-Containing DNIC

Chung-Yen Lu and Wen-Feng Liaw*

Transformation of $\{Fe(NO)_2\}^{10}$ dinitrosyliron complex $Fe(CO)_2(NO)_2$ into $[\{Fe(NO)_2\}^9]_2$ Roussin's red ester $[(\mu\text{-}S(CH_2)_2NH_2)Fe(NO)_2]_2$ triggered by cysteamine via intermediates $[\{Fe(NO)_2\}^{10}]_2[(NO)_2Fe(\mu\text{-}CO)(\mu\text{-}S(CH_2)_2NH_3)Fe(NO)_2] \rightarrow \{Fe(NO)_2\}^9\{Fe(NO)_2\}^{10}[(NO)_2Fe(\mu\text{-}S(CH_2)_2NH_2)(\mu\text{-}S(CH_2)_2NH_3)Fe(NO)_2] \rightarrow [\{Fe(NO)_2\}^9]_2[(\mu\text{-}S(CH_2)_2NH_2)Fe(NO)_2]_2$ is demonstrated.

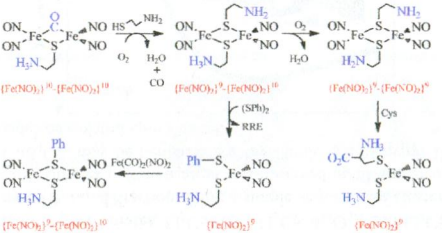

13927 S dx.doi.org/10.1021/ic401451s

Revised Coordination Model and Stability Constants of Cu(II) Complexes of Tris Buffer

Justyna Nagaj, Kamila Stokowa-Sołtys, Ewa Kurowska, Tomasz Frączyk, Małgorzata Jeżowska-Bojczuk, and Wojciech Bal*

Using potentiometry, UV–vis spectroscopy, EPR, and ESI-MS, we developed and thoroughly characterized a complete model of Cu(II)–Tris speciation across a wide span of pH values and for different Cu(II) to Tris ratios. We demonstrated that maximum stoichiometry under any conditions is 2, and deprotonated hydroxyl groups participate directly in Cu(II) binding. Dimeric complexes are formed at neutral pH. Our data provide the basis for using Tris in quantitative Cu(II) research.

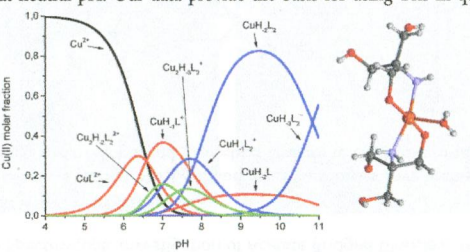

13934 S dx.doi.org/10.1021/ic401577m

Mononuclear Coordination Complexes of Fullerene C_{60} with Zerovalent Cobalt Having $S = 1/2$ Spin State: Co(η^2-C_{60})(L)(C_6H_5CN)·(*o*-$C_6H_4Cl_2$) (L = 1,2-bis(diphenylphosphino)ethane and 1,1′-bis(diphenylphosphino)ferrocene)

Dmitri V. Konarev,* Salavat S. Khasanov, Sergey I. Troyanov, Yoshiaki Nakano, Ksenya A. Ustimenko, Akihiro Otsuka, Hideki Yamochi, Gunzi Saito, and Rimma N. Lyubovskaya

Cobalt coordinates to the 6–6 bonds of C_{60} by η^2-type coordination in mononuclear complexes Co(η^2-C_{60})(dppe)-(C_6H_5CN)·$C_6H_4Cl_2$ (**1**) and Co(η^2-C_{60})(dppf)(C_6H_5CN)·$C_6H_4Cl_2$ (**2**). Additionally, benzonitrile and diphosphine ligands coordinated to cobalt atoms form the distorted square-pyramidal environment around the metal centers. Cobalt atoms have formally a zerovalent state with d^9 electron configuration and $S = 1/2$ spin state. Spins localized on cobalt atoms are magnetically diluted due to long distances between them.

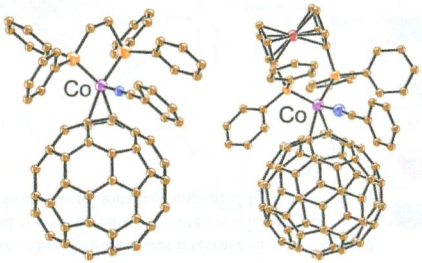

13941 S dx.doi.org/10.1021/ic401582m

Ru(II) and Os(II) Complexes Based on Terpyridyl-Imidazole Ligand Rigidly Linked to Pyrene: Synthesis, Structure, Photophysics, Electrochemistry, and Anion-Sensing Studies

Dinesh Maity, Chanchal Bhaumik, Debiprasad Mondal, and Sujoy Baitalik*

Luminescent bis-tridentate Ru(II) and Os(II) complexes based on terpyridyl-imidazole ligand rigidly linked to pyrene having room temperature lifetimes in the range of 3.8-199.1 ns can act as multichannel sensors for F^-, CN^-, and to some extent for AcO^- ions in solution.

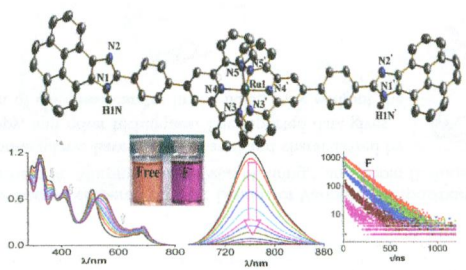

13956 Ⓢ dx.doi.org/10.1021/ic402580n

X-ray Magnetic Circular Dichroism Investigation of the Electron Transfer Phenomena Responsible for Magnetic Switching in a Cyanide-Bridged [CoFe] Chain

Michael L. Baker, Yasutaka Kitagawa, Tetsuya Nakamura, Kou Tazoe, Yasuo Narumi, Yoshinori Kotani, Fumichika Iijima, Graham N. Newton, Mitsutaka Okumura, Hiroki Oshio, and Hiroyuki Nojiri*

The cyanide bridged [CoFe] chain exhibits multifunctional properties via controllable switching between magnetic and diamagnetic phases. Soft X-ray magnetic circular dichroism in conjunction with density functional theory are used to investigate the electron transfer process responsible for this multifaceted behavior.

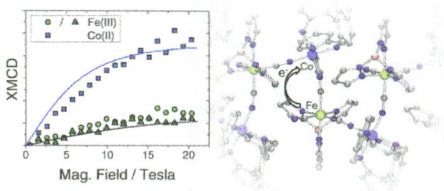

13963 Ⓢ dx.doi.org/10.1021/ic401631e

Structural, Electrochemical, and Spectroscopic Investigation of Acetate Bridged Dinuclear Tetrakis-Schiff Base Macrocycles of Mn and Zn

Subhadeep Kal, Alexander S. Filatov, and Peter H. Dinolfo*

Dinuclear tetrakis-Schiff base macrocycles such as $\mathbf{Mn_2LAc^+}$ and related analogues have been synthesized. To the best of our knowledge, this is the first thorough spectroscopic and theoretical analysis of the higher oxidation states of these or similar complexes.

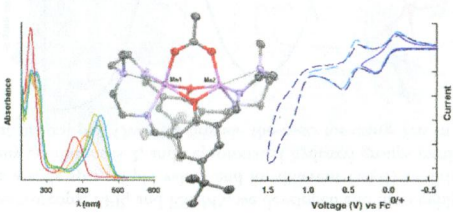

13974 Ⓢ dx.doi.org/10.1021/ic4015724

New Lithium Copper Borates with BO_3 Triangles: $Li_6CuB_4O_{10}$, $Li_3CuB_3O_7$, $Li_8Cu_7B_{14}O_{32}$, and $Li_2Cu_9B_{12}O_{28}$

N. V. Kuratieva, M. Bànki, A. A. Tsirlin, J. Eckert, H. Ehrenberg, and D. Mikhailova*

Crystal structures of three new lithium copper borates, $Li_3CuB_3O_7$, $Li_8Cu_7B_{14}O_{32}$, and $Li_2Cu_9B_{12}O_{28}$, and a new $Li_6CuB_4O_{10}$ polymorph were solved by single-crystal X-ray diffraction. Only a simple sequence of clusters containing corner-sharing BO_3 triangles without any tendency toward complex polymerization was observed in all four structures. The structural features of $Li_3CuB_3O_7$, $Li_8Cu_7B_{14}O_{32}$, and $Li_6CuB_4O_{10}$ may be beneficial for high ionic conductivity. The magnetism of $Li_3CuB_3O_7$ is well-understood in terms of the model of isolated spin dimers.

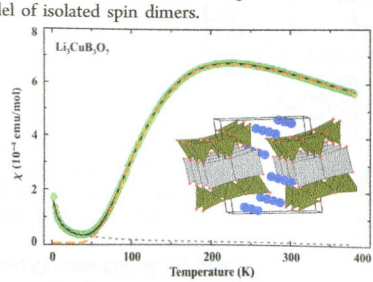

13984 S dx.doi.org/10.1021/ic401662d

DNA/Protein Binding, Molecular Docking, and in Vitro Anticancer Activity of Some Thioether-Dipyrrinato Complexes

Rakesh Kumar Gupta, Gunjan Sharma, Rampal Pandey, Amit Kumar, Biplob Koch, Pei-Zhou Li, Qiang Xu, and Daya Shankar Pandey*

Heteroleptic Ru(II), Rh(III), and Ir(III) complexes containing 5-(4-methylthiophenyl)dipyrromethene have been synthesized and fully characterized. Effective binding of the complexes with DNA and protein has been explored by various physicochemical techniques. The in vitro antitumor activity of complexes were assessed in Dalton's lymphoma (DL) ascite cell lines by MTT assay, acridine orange/ethidium bromide (AO/EtBr) fluorescence staining, and DNA ladder assay.

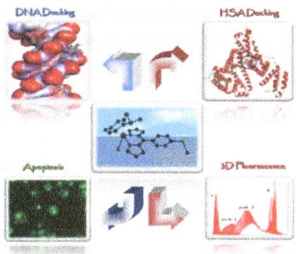

13997 S dx.doi.org/10.1021/ic401676r

Phosphonium Chloromercurate Room Temperature Ionic Liquids of Variable Composition

Andreas Metlen, Bert Mallick, Richard W. Murphy, Anja-Verena Mudring,* and Robin D. Rogers*

A series of phosphonium chloromercurates have been prepared and characterized by ^{199}Hg NMR, Raman spectroscopy, and other techniques. The reported data gives some insight into the speciation of chloromercurates in the liquid state without the presence of other solvents.

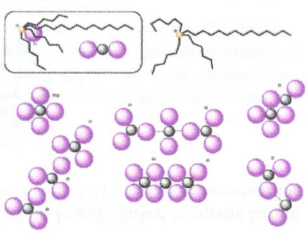

14010 S dx.doi.org/10.1021/ic4017307

Intercalation of Azamacrocyclic Crown Ether into Layered Rare-Earth Hydroxide (LRH): Secondary Host–Guest Reaction and Efficient Heavy Metal Removal

Weili Li, Qingyang Gu, Feifei Su, Yahong Sun, Genban Sun, Shulan Ma,* and Xiaojing Yang

A carboxyethyl substituted azacrown ether derivative was intercalated into a layered gadolinium hydroxide (LGdH), and the prepared composite revealed higher adsorptivity toward transition and heavy metal ions, accompanied by the introduction of nitrate anions.

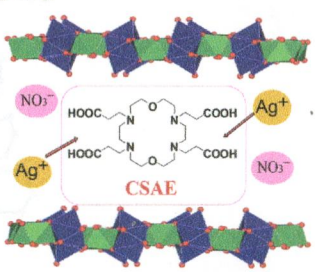

14018 S dx.doi.org/10.1021/ic401765r

Solvent or Temperature Induced Diverse Coordination Polymers of Silver(I) Sulfate and Bipyrazole Systems: Syntheses, Crystal Structures, Luminescence, and Sorption Properties

Li-Yun Du, Wen-Juan Shi, Lei Hou,* Yao-Yu Wang, Qi-Zhen Shi, and Zhonghua Zhu

Three new Ag(I) coordination polymers have been synthesized with Ag_2SO_4 and bipyrazole ligand H_2bpz in different solvents and temperatures; they show diverse structures, luminescence, and adsorption selectivity of CO_2/N_2.

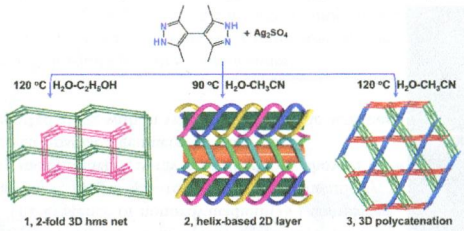

14028 S dx.doi.org/10.1021/ic4017849

Fabrication of Porous Cubic Architecture of ZnO Using Zn-terephthalate MOFs with Characteristic Microstructures

Yu Kimitsuka, Eiji Hosono,* Shintaro Ueno, Haoshen Zhou, and Shinobu Fujihara*

A method for synthesizing porous cubic-shaped ZnO particles a few tens of micrometers in size is described on the basis of a thermal conversion of Zn-terephthalate metal–organic frameworks (MOFs). The resultant ZnO cubes showed intense visible photoluminescence upon irradiation with ultraviolet light.

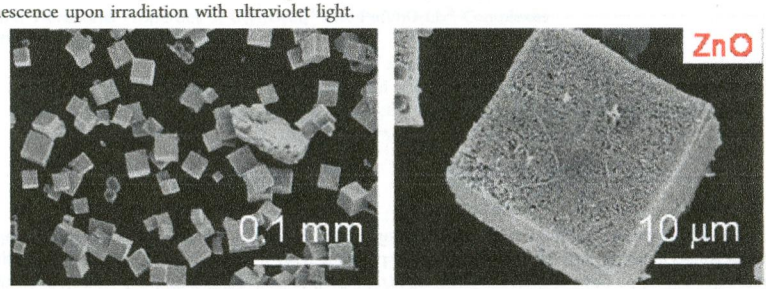

14034 S dx.doi.org/10.1021/ic401804e

Controlled Assembly of Inorganic–Organic Frameworks Based on $[SeMo_6O_{21}]^{4-}$ Polyanion

Donghui Yang, Suzhi Li, Pengtao Ma, Jingping Wang,* and Jingyang Niu*

A series of selenomolybdates have been isolated through rational and deliberate synthetic routes via stereospecific addition of different carboxylic acids.

14040 S dx.doi.org/10.1021/ic4018079

Redox Noninnocence in Coordinated 2-(Arylazo)pyridines: Steric Control of Ligand-Based Redox Processes in Cobalt Complexes

Pradip Ghosh, Subhas Samanta, Suman K Roy, Sucheta Joy, Tobias Krämer, John E. McGrady,* and Sreebrata Goswami*

The steric and electronic properties of 2-(arylazo)pyridine ligands control the oxidation states and coordination geometries of their cobalt complexes. The one-electron-reduced ligand stabilizes Co^{III} either in an $S = 1$ or 0 state, while the oxidized ligand stabilizes Co^{II} in its high-spin configuration.

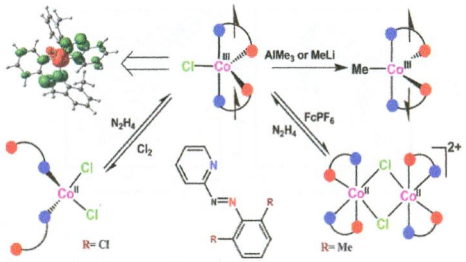

14050 S dx.doi.org/10.1021/ic401837y

Structural and Electronic Properties of Old and New $A_2[M(pin^F)_2]$ Complexes

Laleh Tahsini, Sarah E. Specht, June S. Lum, Joshua J. M. Nelson, Alexandra F. Long, James A. Golen, Arnold L. Rheingold, and Linda H. Doerrer*

New $A_2[M(pin^F)_2]$ complexes of Fe–Zn were prepared, fully characterized, and compared with related literature species. All Ni and Cu complexes exhibit square-planar geometry, but Fe or Co geometries are cation dependent. Zn species are consistently tetrahedral. Solvent binding to Co is cation independent, but only observed with Ni complexes having noncoordinating cations. Cyclic voltammetry studies reveal reversible M(III)/M(II) couples for Ni and Cu and quasi-reversible couples for Fe and Co complexes.

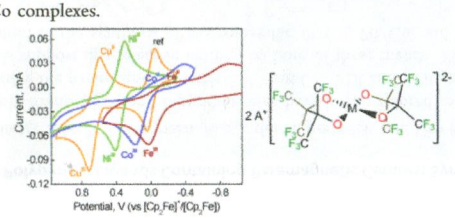

14064 S dx.doi.org/10.1021/ic401851z

Zwitterionic Weak-Link Approach Complexes Based on Anionic Icosahedral Monocarbaboranes

Robert D. Kennedy, Charlotte L. Stern, and Chad A. Mirkin*

The anionic hemilabile phosphinothioether ligand, $[1\text{-}(Ph_2PCH_2CH_2S)\text{-}closo\text{-}1\text{-}CB_{11}H_{11}]^-$, was used to synthesize a family of zwitterionic Weak-Link Approach (WLA) complexes of platinum(II), palladium(II), and rhodium(I). The chelating strength of the ligand is comparable to that of hemilabile ligands that contain the electron-rich B-bound *closo*-1,7-$C_2B_{10}H_{11}$ moiety, thus demonstrating the use of charge to influence ligand coordination strength. An unprecedented type of salt is described, in which the anion and cation are mutually isostructural and isoelectronic Rh(I) complexes.

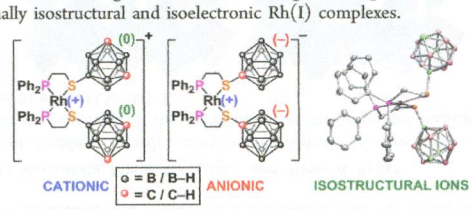

14072 S dx.doi.org/10.1021/ic401858s

Density Functional Study for the Bridged Dinuclear Center Based on a High-Resolution X-ray Crystal Structure of ba_3 Cytochrome *c* Oxidase from *Thermus thermophilus*

Wen-Ge Han Du and Louis Noodleman*

DFT OLYP calculations have been performed on the $Fe_{a3}\cdots O1{-}O2\cdots Cu_B$ dinuclear center (DNC) of the X-ray crystal structure (PDB code: 3S8G) of ba_3 cytochrome *c* oxidase from *Thermus thermophilus*. We propose that the dioxygen species observed in 3S8G is best represented by HO_2^- and the DNC of this crystal structure represents the superposition of the $Fe_{a3}^{2+}{-}(HO_2^-){-}Cu_B^+$ DNC's in different states (Fe^{2+} in low spin (LS), intermediate spin (IS), or high spin (HS)) with the majority species having the proton of the HO_2^- residing on the oxygen atom (O1) which is closer to the Fe_{a3}^{2+} site.

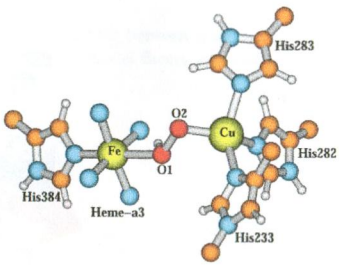

14089 S dx.doi.org/10.1021/ic4018486

Coordination of Lead(II) in the Supramolecular Environment Provided by a "Two-Story" Calix[6]arene-based N_6 Ligand

Diana Over, Xianshun Zeng, Claudia Bornholdt, Jérôme Marrot, and Olivia Reinaud*

A "two-story" calix[6]arene presenting a N_6 cryptand site allows strong complexation of Pb^{II} ions while maintaining a free site open to a guest molecule. A subtle combination of flexibility/geometrical constraints imposed by the calixarene core allows PbII binding in a hemispherical environment. Guests such as H_2O or EtOH interact with the metal center and the calix core. Although electrostatic, these interactions are strong enough for the host–guest complexes to be observed in solution.

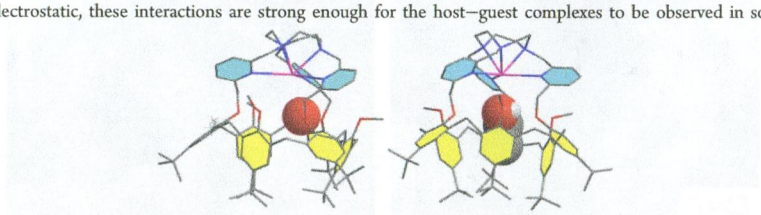

14096 S dx.doi.org/10.1021/ic401866x

Highly Stable Hexacoordinated Nonoxidovanadium(IV) Complexes of Sterically Constrained Ligands: Syntheses, Structure, and Study of Antiproliferative and Insulin Mimetic Activity

Subhashree P. Dash, Sagarika Pasayat, Saswati Bhakat, Satabdi Roy, Rupam Dinda,* Edward R. T. Tiekink, Subhadip Mukhopadhyay, Sujit K. Bhutia, Manasi R. Hardikar, Bimba N. Joshi, Yogesh P. Patil, and M. Nethaji

Three highly stable, hexacoordinated nonoxo vanadium(IV), $V^{IV}(L)_2$, complexes have been isolated and structurally characterized with tridentate aroylhydrazonates containing ONO donor atoms. The existence of nonoxovanadium(IV) complexes was confirmed by elemental analysis, ESI mass spectroscopy, cyclic voltammetry, EPR, and magnetic susceptibility measurements. X-ray crystallography showed the N_3O_3 donor set to define a trigonal prismatic geometry in each case. Antiproliferative activities are reported along with in vitro insulin mimetic activities.

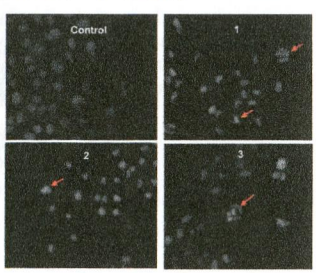

14108 S dx.doi.org/10.1021/ic401917h

High-Pressure Synthesis, Crystal Structure, and Properties of In_2NiMnO_6 with Antiferromagnetic Order and Field-Induced Phase Transition

Wei Yi,* Qifeng Liang, Yoshitaka Matsushita, Masahiko Tanaka, and Alexei A. Belik*

In_2NiMnO_6 extends the family of double rare-earth perovskites R_2NiMnO_6 (R = rare earth, Y) to smaller R ions. We investigate its structure and magnetic properties. It shows distinct magnetic properties, including antiferromagnetism below 26 K and a field-induced transition from 18 kOe at 5 K.

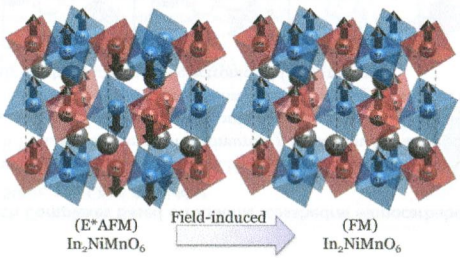

14116 S dx.doi.org/10.1021/ic401952s

Heterobimetallic Complexes of Polypyridyl Ligands Containing Paramagnetic Centers: Synthesis and Characterization by IR and EPR

Sarah K. Goforth, Richard C. Walroth, Joseph A. Brannaka, Alexander Angerhofer, and Lisa McElwee-White*

Ligands containing linked dipicolylamine (dpa) and bipyridine sites have been explored as platforms for the synthesis of heterometallic complexes containing the paramagnetic metals Cu^{2+} and Co^{2+}. IR and EPR studies on the bimetallic complexes and simplified model compounds support dpa-selective binding by both of these metals. The binding preferences have been used to control selective metalation in the synthesis of heterometallic Pt/Cu, Pd/Cu, and Rh/Cu complexes.

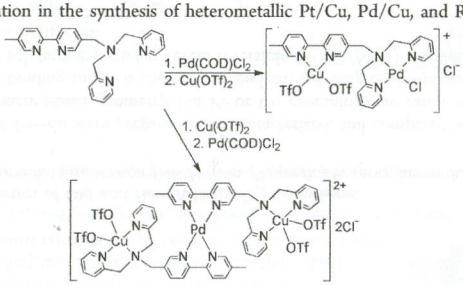

14124 (S) dx.doi.org/10.1021/ic401948p

Solventless Supramolecular Chemistry via Vapor Diffusion of Volatile Small Molecules upon a New Trinuclear Silver(I)-Nitrated Pyrazolate Macrometallocyclic Solid: An Experimental/Theoretical Investigation of the Dipole/Quadrupole Chemisorption Phenomena

Rossana Galassi,* Simone Ricci, Alfredo Burini, Alceo Macchioni, Luca Rocchigiani, Fabio Marmottini, Sammer M. Tekarli, Vladimir N. Nesterov, and Mohammad A. Omary*

A new cyclic trinuclear silver(I) derivative, tris[μ-(3,5-dinitropyrazolato]silver(I)), shows unprecedented reversible chemisorption properties toward vapors of small inorganic and organic molecules bearing N, S, or O donor atoms. The adducts are stable in the solid state but dissociate in solution. Computational results rationalize the experimental data, ascribing the phenomenon to strong quadrupole–dipole interactions.

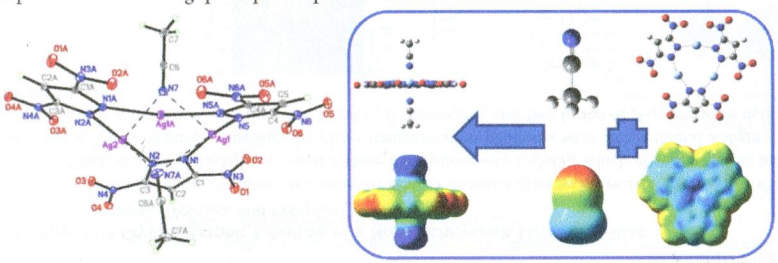

14138 (S) dx.doi.org/10.1021/ic401991n

Structural and Vibrational Properties of $U(VI)O_2Cl_4^{2-}$ and $Pu(VI)O_2Cl_4^{2-}$ Complexes

David D. Schnaars and Richard E. Wilson*

Because the symmetric and asymmetric vibrational modes of actinyl ions are sensitive to the number and identity of equatorially coordinated ligands, the structural and vibrational properties of an isostructural series of $U(VI)O_2Cl_4^{2-}$ and $PuO_2Cl_4^{2-}$ complexes have been studied to investigate these effects among two differing actinyl(VI) ions.

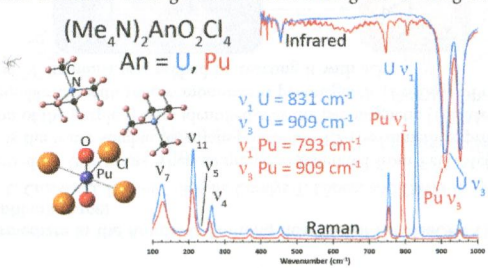

14148 dx.doi.org/10.1021/ic402010h

Pressure-Induced Local Lattice Distortions in α-Co[N(CN)$_2$]$_2$

J. L. Musfeldt,* T. V. Brinzari, J. A. Schlueter, J. L. Manson, A. P. Litvinchuk, and Z. Liu

Transition metal dicyanamides are ideal physical platforms with which to investigate the use of external stimuli to manipulate the properties. By bringing together diamond anvil cell techniques, vibrational spectroscopies, and dynamics calculations, we reveal the lattice distortions associated with the pressure-induced ferromagnetic → antiferromagnetic crossover in Co[N(CN)$_2$]$_2$. These findings advance the microscopic understanding of magnetoelastic coupling in molecule-based materials as well as higher energy scale systems like the oxides.

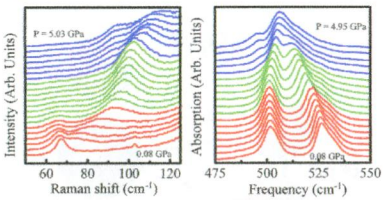

14155 dx.doi.org/10.1021/ic402012d

Graphite Oxide/Metal–Organic Framework (MIL-101): Remarkable Performance in the Adsorptive Denitrogenation of Model Fuels

Imteaz Ahmed, Nazmul Abedin Khan, and Sung Hwa Jhung*

A highly porous metal–organic framework (MOF), MIL-101 (Cr-benzenedicarboxylate), was synthesized in the presence of graphite oxide (GO) to produce GO/MIL-101 composites. The GO/MIL-101 composite has the highest adsorption capacity for nitrogen-containing compounds such as indole from model fuels among reported adsorbents so far, partly because of the increased porosity of the composite.

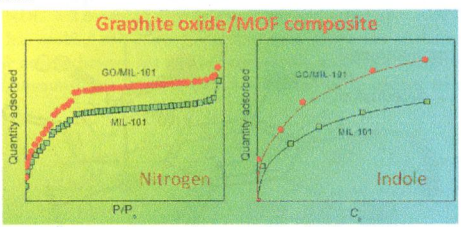

14162 dx.doi.org/10.1021/ic4020493

Synthesis and Properties of Uranium Sulfide Cations. An Evaluation of the Stability of Thiouranyl, {S=U=S}$^{2+}$

Cláudia C. L. Pereira, Maria del Carmen Michelini,* Joaquim Marçalo,* Yu Gong, and John K. Gibson

The U^{2+} ion reacted with the facile sulfur-atom donor OCS to produce US_2^{2+} in the gas phase. Density functional theory computations indicate that, in contrast to uranyl, the linear thiouranyl isomer is higher in energy than the ground-state side-on η^2-S_2 triangular isomer.

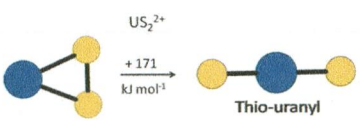

14168 S dx.doi.org/10.1021/ic402056k

Ammonium Tetrathiomolybdate: A Versatile Catalyst for Hydrogen Evolution Reaction from Water under Ambient and Hostile Conditions

Sudipta Chatterjee, Kushal Sengupta, Subal Dey, and Abhishek Dey*

Ammonium tetrathiomolybdate is an efficient catalyst for HER under ambient conditions with almost no overpotential. Because of a possible ligand based H_2 generation mechanism, HER activity remains unperturbed in water containing O_2, CO, and H_2S, as well as in sea water.

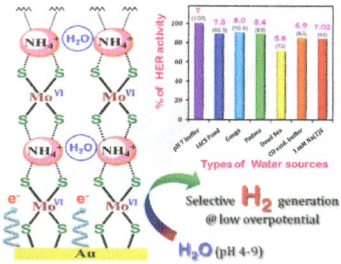

14178 S dx.doi.org/10.1021/ic402081q

Characterization of an Intermediate in the Ammonia-Forming Reaction of Fe(DMeOPrPE)$_2$N$_2$ with Acid (DMeOPrPE = 1,2-[bis(dimethoxypropyl)phosphino]ethane)

Chantal G. Balesdent, Justin L. Crossland, Daniel T. Regan, Coralys T. López, and David R. Tyler*

The short-lived purple intermediate that forms when ammonia is generated from Fe(DMeOPrPE)$_2$N$_2$ and acid was characterized. (DMeOPrPE is the water-soluble bidentate phosphine 1,2-[bis(dimethoxypropyl)phosphino]ethane.) Spectroscopic characterization of the purple species identified it as the paramagnetic $[((DMeOPrPE)_2Fe)_2(\mu\text{-}N_2)]^{2+}$ complex. This purple dimer exists in equilibrium with yellow, monomeric, paramagnetic $[Fe(DMeOPrPE)_2N_2]^+$. The role of the purple intermediate in the formation of ammonia was probed by reacting it with acid.

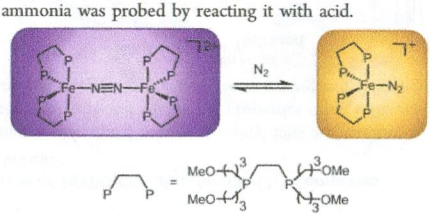

14188 dx.doi.org/10.1021/ic402112z

In Situ High-Temperature Crystallographic Evolution of a Nonstoichiometric Li_2O-$2SiO_2$ Glass

Saifang Huang, Zhaohui Huang, Wei Gao, and Peng Cao*

The high-temperature crystallographic evolution in a complex lithium disilicate glass was investigated by synchrotron powder diffraction. The structural change of $Li_2Si_2O_5$ showed a close correlation with Li_2SiO_3, which gives an insight into the nucleation mechanism. Upon heating or cooling, the phase transformation processes were different, and a slight difference in change rates of their unit cell volume was observed. Li_2SiO_3, β-cristobalite, and two forms of β-quartz were detected during cooling rather than $Li_2Si_2O_5$.

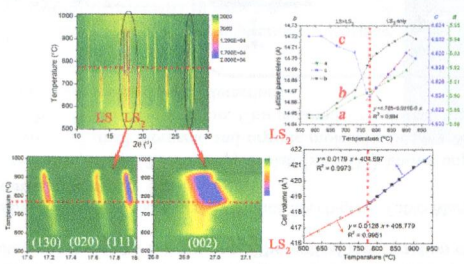

14196 dx.doi.org/10.1021/ic402124s

XRD Monitoring of α Self-Irradiation in Uranium–Americium Mixed Oxides

Denis Horlait, Florent Lebreton, Pascal Roussel, and Thibaud Delahaye*

Evolutions of $U_{1-x}Am_xO_{2\pm\delta}$ ($0.075 \leq x \leq 0.5$) solid solutions were monitored by XRD. The five samples studied showed similar behavior: (1) an initial oxidation under air, (2) stabilization of the fluorite structure and its good resistance to self-irradiation, (3) structural swelling due to ^{241}Am α self-irradiation up to 0.8–0.9% volume increase, and (4) very limited evolutions of microstrain and crystallite size.

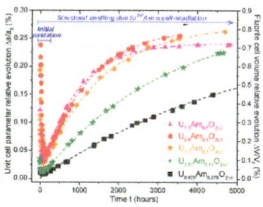

14205 dx.doi.org/10.1021/ic4021349

Theoretical ^{57}Fe Mössbauer Spectroscopy for Structure Elucidation of [Fe] Hydrogenase Active Site Intermediates

Joël Gubler, Arndt R. Finkelmann, and Markus Reiher*

A new relativistic approach for the general calculation of Mössbauer parameters has been developed and applied to active-site models of [Fe] hydrogenase. The resting state and the protonation states of proton acceptors in the vicinity of the catalytic Fe atom are identified.

relativistic DFT → Mössbauer parameters → structure

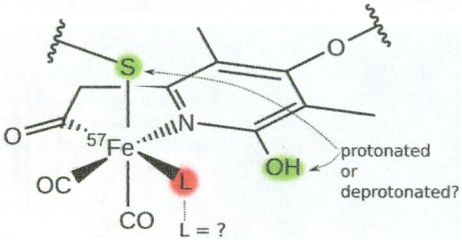

14216 dx.doi.org/10.1021/ic4021355

Synthesis and Characterization of the Titanium Bisamide Ti{N(H)Ar^{iPr_6}}$_2$ (Ar^{iPr_6} = C_6H_3-2,6-(C_6H_2-2,4,6-$^iPr_3$)$_2$ and Its TiCl{N(H)Ar^{iPr_6}}$_2$ Precursor: Ti(II) → Ti(IV) Cyclization

Jessica N. Boynton, Jing-Dong Guo, Fernande Grandjean, James C. Fettinger, Shigeru Nagase, Gary J. Long, and Philip P. Power*

Whereas the bulky terphenyl amido ligand -N(H)Ar^{iPr_6} supports linear coordination in the metal(II) series M{N(H)Ar^{iPr_6}}$_2$ (M = V → Ni), the synthesis of the corresponding Ti{N(H)Ar^{iPr_6}}$_2$ (pictured) shows that it undergoes a metal-ring cyclization to produce a Ti(IV) product.

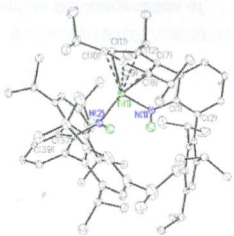

14224 (S) dx.doi.org/10.1021/ic4021564

$VSb(SeO_3)_4$, First Selenite Containing V^{3+} Cation: Synthesis, Structure, Characterization, Magnetic Properties, and Calculations

Yiseul Shin, Dong Woo Lee, Kwang Yong Choi, Hyun-Joo Koo, and Kang Min Ok*

A new vanadium(III) antimony(V) selenite, $VSb(SeO_3)_4$, has been synthesized by a standard solid-state reaction. The effective magnetic moment is estimated to be $\mu_{eff} = 2.57\ \mu_B$.

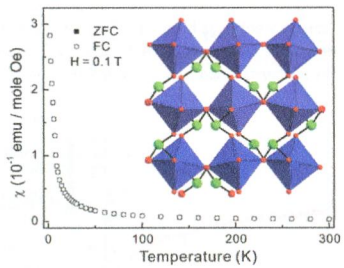

14231 (S) dx.doi.org/10.1021/ic402159y

Intramolecular Phosphorus–Phosphorus Bond Formation within a Co_2P_4 Core

Tianshu Li, Nicholas Arleth, Michael T. Gamer, Ralf Köppe, Timo Augenstein, Fabian Dielmann, Manfred Scheer, Sergey N. Konchenko, and Peter W. Roesky*

The reduction of $[(Cp'''Co)_2(\mu,\eta^{2:2}\text{-}P_2)_2]$ with the samarocenes, $[(C_5Me_4R)_2Sm(THF)_n]$, gives $[(Cp'''Co)_2P_4Sm(C_5Me_4R)_2]$. These are the first examples of intramolecular P–P coupling in a polyphosphide complex after reduction of the transition metal.

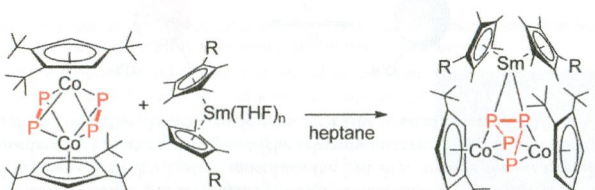

R = Me, n = 2;
R = Propyl, n = 0

R = Me; Propyl

14237 Ⓢ dx.doi.org/10.1021/ic402170q

Oxidation States, Geometries, and Electronic Structures of Plutonium Tetroxide PuO_4 Isomers: Is Octavalent Pu Viable?
Wei Huang, Wen-Hua Xu, Jing Su, W. H. E. Schwarz, and Jun Li*

PuO_4 may exist, though hardly as a homolog of tetrahedral OsO_4, as repeatedly speculated. The exotic low-spin high-oxidation state of Pu(VIII) is highly unstable against intramolecular electron transfer. The more common plutonyl(V)$^+$ unit may be loosely coupled to a superoxido O_2^- ligand, forming PuO_4 as a high-spin complex of lower oxidation state, $^5C_{2v}$-$(PuO_2)^+(O_2)^-$ (see figure). The leading valence configuration with open electron shells on plutonium, $(f^3)Pu^{5+}$, and dioxygen, $(\pi^{*3})O_2^-$, yields a highly correlated valence electronic system. From uranium onward, the highest oxidation states of the actinides become more and more unlikely.

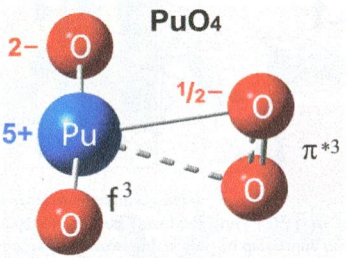

14246 Ⓢ dx.doi.org/10.1021/ic402173z

Electronic, Optical, and Computational Studies of a Redox-Active Napthalenediimide-Based Coordination Polymer
Chanel F. Leong, Bun Chan, Thomas B. Faust, Peter Turner, and Deanna M. D'Alessandro*

A dual experimental and computational approach to the novel one-dimensional coordination framework $(Zn(DMF)\text{-}NO_3)_2(NDC)(DPMNI)$, where NDC = 2,6-naphthalenedicarboxylate and DPMNI = *N*,*N*′-bis(4-pyridylmethyl)-1,4,5,8-naphthalenetetracarboxydiimide, has enabled the electronic and spectral properties of the neutral, monoradical anion, and dianion states to be elucidated. A new technique for in situ vis−near-IR solid-state spectroelectrochemistry, in addition to light-activated EPR spectroscopy, demonstrates that the radical states can be generated via electrical and light stimuli.

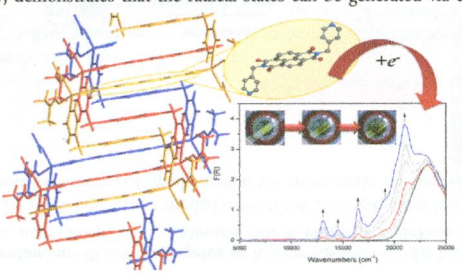

14253 S dx.doi.org/10.1021/ic402202w

Metal–Metal Interaction in Fischer Carbene Complexes: A Study of Ferrocenyl and Biferrocenyl Tungsten Alkylidene Complexes

Belinda van der Westhuizen, J. Matthäus Speck, Marcus Korb, Joachim Friedrich, Daniela I. Bezuidenhout,* and Heinrich Lang*

The syntheses, structures, and UV–vis-NIR spectroelectrochemical analyses of novel mono- and biscarbene tungsten complexes of ferrocene and biferrocene are presented. The order of the different oxidation processes could be established, while the NIR spectra recorded provided evidence for the first time for charge transfer metal–metal interaction between the mixed-valent tungsten(0) pentacarbonyl moieties and the ferrocenyl/biferrocenyl carbene substituents. This was confirmed with the spectroelectrochemical investigation and by use of density functional theory calculations.

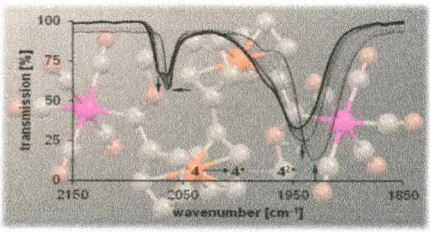

14264 S dx.doi.org/10.1021/ic402205j

pH-Responsive Lanthanide Complexes Based on Reversible Ligation of a Diphenylphosphinamide

Marco Giardiello, Mauro Botta, and Mark P. Lowe*

Gd/Eu-DO3A-based complexes bearing a pendant diphenylphosphinamide exhibit pH-responsive reversible ligation of the phosphinamide. The pH dependence of this ligation modulates the hydration state of the complexes: in acidic media, the phosphinamide is not coordinated, hydration state $q = 2$ [the relaxivity increases (Gd) and the emission intensity decreases (Eu)]; in basic media, coordination of the phosphinamide gives $q = 1$ [the relaxivity decreases (Gd) and the emission intensity (Eu) increases].

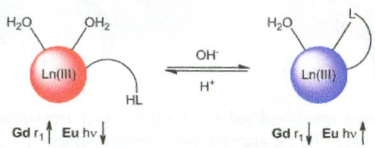

14270 S dx.doi.org/10.1021/ic402213s

Crystal Structure and Cyclic Hydrogenation Property of Pr_4MgNi_{19}

Kenji Iwase,* Naoyoshi Terashita, Kazuhiro Mori, Hitoshi Yokota, and Tetsuya Suzuki

The cyclic absorption–desorption property of Pr_4MgNi_{19} indicated that the retention rates were 94%, 92%, 91%, and 90% after 250, 500, 750, and 1000 cycles.

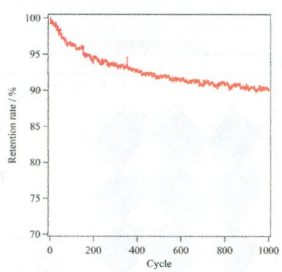

14275 dx.doi.org/10.1021/ic4022189

Clusters $[M_a(GaCp^*)_b(CNR)_c]$ (M = Ni, Pd, Pt): Synthesis, Structure, and Ga/Zn Exchange Reactions

Mariusz Molon, Katharina Dilchert, Christian Gemel, Rüdiger W. Seidel, Julian Schaumann, and Roland A. Fischer*

Reactions of homoleptic isonitrile ligated d^{10}-metal clusters with GaCp* lead the formation of heteroleptic, tri- and tetranuclear clusters. These reactions involve isonitrile substitution reactions, GaCp* addition reactions and cluster formation reactions. Investigations of these on Ga/Zn exchange reactions lead to the tetranuclear Zn-rich clusters. The electronic situation and geometrical arrangement of atoms of all fully characterized compounds will be presented and discussed.

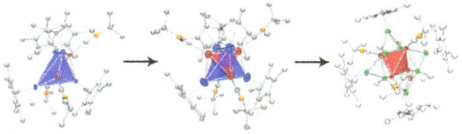

14284 dx.doi.org/10.1021/ic402233g

Lanthanide(III) Complexes of Rhodamine–DO3A Conjugates as Agents for Dual-Modal Imaging

Charlotte Rivas, Graeme J. Stasiuk, Juan Gallo, Florencia Minuzzi, Guy A. Rutter, and Nicholas J. Long*

Two new dual-modal MRI/optical probes based on a rhodamine–DO3A conjugate have been synthesized, and one of them displays an off–on pH switch upon its preferential uptake within the more acidic microenvironment of tumor cells.

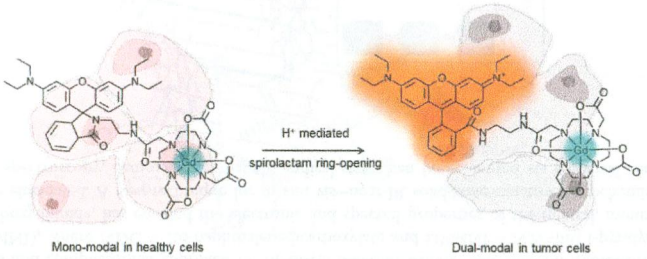

14294 dx.doi.org/10.1021/ic402254q

Exchanging Conformations of a Hydroformylation Catalyst Structurally Characterized Using Two-Dimensional Vibrational Spectroscopy

Matthijs R. Panman, Jannie Vos, Vladica Bocokić, Rosalba Bellini, Bas de Bruin, Joost H. N. Reek, and Sander Woutersen*

"Frozen fluxionality": Two-dimensional infrared spectroscopy is used to determine bond angles in the two rapidly exchanging solution conformations of the hydroformylation catalyst (xantphos)$Rh(CO)_2H$. In one of the conformations, the OC–Rh–CO angle deviates significantly from the canonical value.

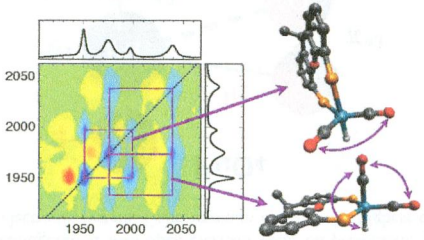

14299 S

dx.doi.org/10.1021/ic402276e

$Ba_4Ta_2O_9$ Oxide Prepared from an Oxalate-Based Molecular Precursor—Characterization and Properties

Lidija Androš, Marijana Jurić,* Jasminka Popović, Ana Šantić, Predrag Lazić, Metka Benčina, Matjaz Valant, Nevenka Brničević, and Pavica Planinić

Thermal treatment of the novel oxalate-based compound $\{Ba_2(H_2O)_5[TaO(C_2O_4)_3]HC_2O_4\}\cdot H_2O$ (**1**), used as a single-source precursor, up to 1200 °C leads to the mixed-metal γ-$Ba_4Ta_2O_9$ phase. The spectroscopic, optical, photocatalytic, and electrical properties of this oxide, having the 6*H*-perovskite structure, are investigated. An absorption spectrum and band structure of the γ-$Ba_4Ta_2O_9$ are also calculated.

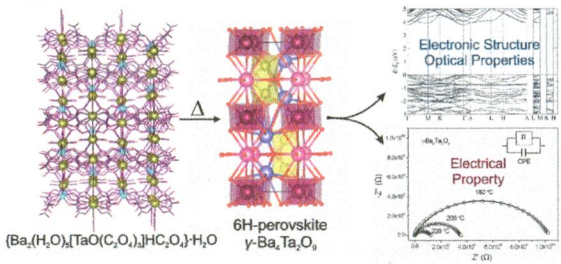

14309 S

dx.doi.org/10.1021/ic402278c

Synthetic and Coordination Chemistry of the Heavier Trivalent Technetium Binary Halides: Uncovering Technetium Triiodide

Erik V. Johnstone,* Frederic Poineau, Jenna Starkey, Thomas Hartmann, Paul M. Forster, Longzhou Ma, Jeremy Hilgar, Efrain E. Rodriguez, Romina Farmand, Kenneth R. Czerwinski, and Alfred P. Sattelberger

Technetium triiodide, the first technetium iodide reported, was obtained from the reaction of $Tc_2(O_2CCH_3)_4Cl_2$ with flowing HI(g) at elevated temperatures and from the reaction of technetium metal and elemental iodine in a sealed tube at 400 °C. Similarly, technetium tribromide was synthesized from the reaction of $Tc_2(O_2CCH_3)_4Cl_2$ with flowing HBr(g) at elevated temperatures. The structures of both $TcBr_3$ and TcI_3 consist of face-sharing TcX_6 octahedra, which is consistent with other triiodides and tribromides of molybdenum and ruthenium. The thermal stabilities of $TcBr_3$ and TcI_3 were studied under vacuum at elevated temperatures.

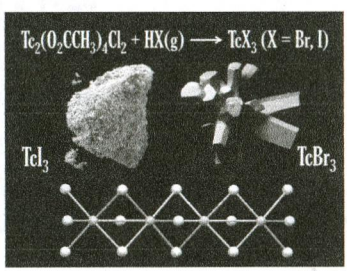

14317 Ⓢ dx.doi.org/10.1021/ic402297f

Selective $4e^-/4H^+$ O_2 Reduction by an Iron(tetraferrocenyl)Porphyrin Complex: From Proton Transfer Followed by Electron Transfer in Organic Solvent to Proton Coupled Electron Transfer in Aqueous Medium

Kaustuv Mittra, Sudipta Chatterjee, Subhra Samanta, and Abhishek Dey*

An iron porphyrin catalyst bearing four ferrocenes and a hydrogen bonding distal pocket is found to catalyze $4e^-/4H^+$ oxygen reduction reaction (ORR) in organic solvent under homogeneous conditions in the presence of 2–3 equiv of Trifluoromethanesulphonic acid. Absorption spectroscopy, EPR, and resonance Raman data along with H_2O_2 assay indicate that one out of the four electrons necessary to reduce O_2 to H_2O is donated by the ferrous porphyrin while three are donated by the distal ferrocene residues.

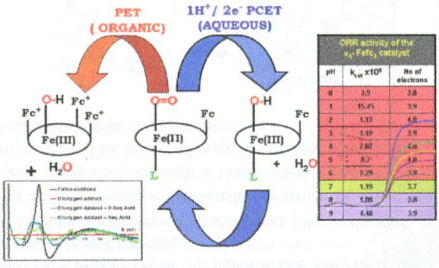

14326 Ⓢ dx.doi.org/10.1021/ic402266j

Solution-Based Synthesis of GeTe Octahedra at Low Temperature

Stephan Schulz,* Stefan Heimann, Kevin Kaiser, Oleg Prymak, Wilfried Assenmacher, Jörg Thomas Brüggemann, Bert Mallick, and Anja-Verena Mudring

Crystalline GeTe octahedra were obtained from the reaction of $GeCl_2$·dioxane and $Te(SiEt_3)_2$ in different organic solvents at low temperature and characterized by SEM, TEM, EDX, and XRD. The solvents critically influence the reaction mechanism, and oleylamine serves rather as a reagent than as a simple capping agent. The role of reaction time, reaction temperature, and precursor concentration on the GeTe particle formation is shown. In addition, the single-crystal X-ray structure of GeTe is reported.

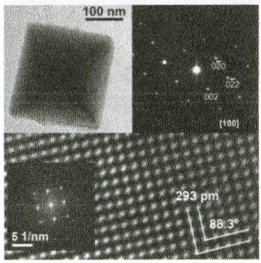

14334 Ⓢ dx.doi.org/10.1021/ic4023344

Kinetic and DFT Studies on the Mechanism of C−S Bond Formation by Alkyne Addition to the $[Mo_3S_4(H_2O)_9]^{4+}$ Cluster

Jose Ángel Pino-Chamorro, Andrés G. Algarra, M. Jesús Fernández-Trujillo, Rita Hernández-Molina, and Manuel G. Basallote*

On the basis of stopped-flow experiments and theoretical calculations, a mechanism is proposed for the reaction of $[Mo_3S_4(H_2O)_9]^{4+}$ with alkynes leading to formation of two C−S bonds between the alkyne and two of the bridging sulfides. The reaction occurs in a single kinetic step with lateral approach of the alkyne to the cluster to allow for the simultaneous formation of both C−S bonds, the metal centers playing a passive role despite reactions at those sites being well illustrated for this kind of cluster.

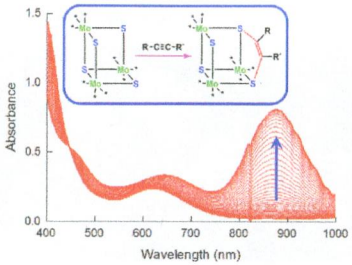

14343 Ⓢ dx.doi.org/10.1021/ic402342y

Heteroleptic Silver(I) Complexes Prepared from Phenanthroline and Bis-phosphine Ligands

Adrien Kaeser, Béatrice Delavaux-Nicot,* Carine Duhayon, Yannick Coppel, and Jean-François Nierengarten*

The heteroleptic coordination scenario of silver(I) with various phenanthroline ligands (NN) and different bis-phosphine (PP) derivatives has been investigated. In addition to the X-ray crystal structural characterization of the resulting mixed ligand Ag(I) complexes, detailed NMR studies have been performed to disclose the behavior of the prepared silver(I) complexes in solution.

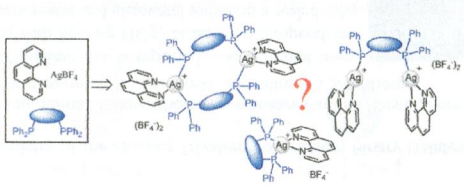

14355 S dx.doi.org/10.1021/ic4024025

Extremely Long Cu···O Contact as a Possible Pathway for Magnetic Interactions in $Na_2Cu(CO_3)_2$

Yulia V. Nelyubina,* Alexander A. Korlyukov, Ivan V. Fedyanin, and Konstantin A. Lyssenko

Chemical binding in crystalline $Na_2Cu(CO_3)_2$, showing ferromagnetic intralayer exchange and weak antiferromagnetic interlayer coupling, was examined within the topological analysis of experimental and theoretical electron density functions in its crystal. Together with modeling of a superexchange pathway, the results obtained reveal a very weak Cu···O interaction (0.5 kcal/mol worth) between the copper−carbonate layers that is nevertheless bonding and may serve as a possible pathway for antiferromagnetic interactions.

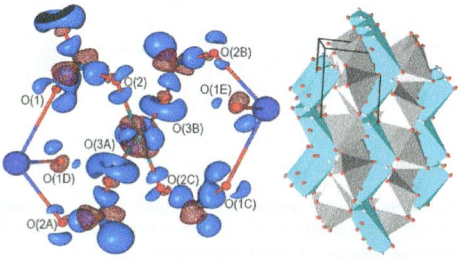

14364 S dx.doi.org/10.1021/ic402455x

Synthesis, Crystal Structure, and High Temperature Transport Properties of *p*-Type $Cu_2Zn_{1-x}Fe_xSnSe_4$

Yongkwan Dong, Hsin Wang, and George S. Nolas*

An investigation into Fe substituted $Cu_2Zn_{1-x}Fe_xSnSe_4$ stannites was initiated. These compounds form in the tetragonal stannite structure type. The Fe content directly impacts the transport properties. $Cu_2Zn_{0.4}Fe_{0.6}SnSe_4$ has a ZT value of 0.46 at 800 K, the highest ZT value thus far reported for Fe-doped compositions in this material system.

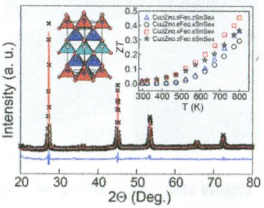

14368 S dx.doi.org/10.1021/ic4024629

Synthesis, Structures, and Luminescence Properties of Interconvertible $Au^I_2Zn^{II}$ and $Au^I_3Zn^{II}$ Complexes with Mixed Bis(diphenylphosphino)methane and D-Penicillaminate

Yuji Hashimoto, Nobuto Yoshinari, Daisuke Naruse, Koichi Nozaki, and Takumi Konno*

A trinuclear $Au^I_2Zn^{II}$ cyclic complex with an 8-membered metalloring structure, $[\{Au_2(dppm)\}\{Zn(D\text{-}pen)_2\}]$, was reversibly expanded to the tetranuclear $Au^I_3Zn^{II}$ cyclic complex with a 12-membered metalloring structure, $[\{Au_3(dppm)_2\}\{Zn(D\text{-}pen)_2\}]^+$, by adding an $\{Au(dppm)\}^+$ unit. The Au^I−Zn^{II} complexes show photoluminescence with different color and brightness, by changing intramolecular aurophilic interactions.

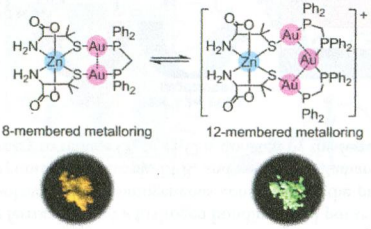

14376 S dx.doi.org/10.1021/ic402478h

Nonelectrochemical Synthesis, Crystal Structure, and Physical Properties of the Radical Salt $[ET]_2[CuCl_4]$ (ET = Bis(ethylenedithio)tetrathiafulvalene)

Bárbara Rodríguez-García, Sara Goberna-Ferrón, Yong-Sung Koo, Jordi Benet-Buchholz, and José Ramón Galán-Mascarós*

Reaction of the organic radical bis(ethylenedithio)tetrathiafulvalene (ET) with a polynuclear copper anion $[Cu_4OCl_{10}]^{4-}$ yields single crystals of the radical salt $[ET]_2[CuCl_4]$, that contains organic radical dimers with strong magnetic superexchange.

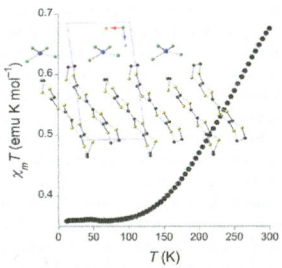

14382 S dx.doi.org/10.1021/ic402523v

Lanthanide Complexes Based on β-Diketonates and a Tetradentate Chromophore Highly Luminescent as Powders and in Polymers

Eugen S. Andreiadis, Nicolas Gauthier, Daniel Imbert, Renaud Demadrille, Jacques Pécaut, and Marinella Mazzanti*

The use of the anionic tetradentate terpyridine-carboxylate ligand in combination with two β-diketonates ligands leads to a ternary Eu(III) complex with high stability with respect to ligand dissociation in solution, extended absorption window toward the visible region (390 nm), and high luminescence quantum yield in the solid state (Φ = 66%). Furthermore, this complex has been incorporated in polymer matrixes leading to highly luminescent flexible layers (62%).

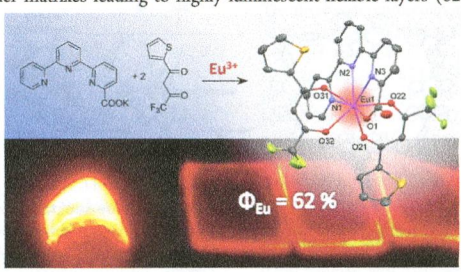

14391 S dx.doi.org/10.1021/ic4025475

Thermochemical and Mechanistic Studies of Electrocatalytic Hydrogen Production by Cobalt Complexes Containing Pendant Amines

Eric S. Wiedner,* Aaron M. Appel, Daniel L. DuBois, and R. Morris Bullock*

Cobalt complexes containing tetradentate phosphine ligands with pendant proton relays were found to be active electrocatalysts for the production of hydrogen. The H−Co bond energetics of potential intermediates were explored by experiment and computation. These studies suggest that H_2 is formed by heterocoupling of a cobalt(II) hydride ligand with a protonated pendant amine.

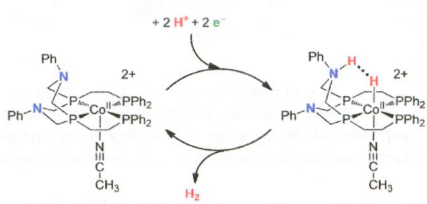

14404 S dx.doi.org/10.1021/ic402600h

Phenylcyanamide Ligand Control of Photo-Induced Linkage Isomerism

Mohommad M. R. Choudhuri and Robert J. Crutchley*

The electron donor properties of the phenylcyanamide ligand can be used to control the photoinduced and electrochemically generated linkage isomerism of $[Ru(bpy)_2(L)(dmso\text{-}S)]^+$ complexes.

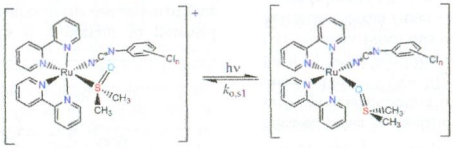

14411 S dx.doi.org/10.1021/ic4026975

Hybrid Nanomaterials: Anchoring Magnetic Molecules on Naked Gold Nanocrystals

Rebecca J. Holmberg, Amy-Jayne Hutchings, Fatemah Habib, Ilia Korobkov, Juan C. Scaiano, and Muralee Murugesu*

Through adhering lanthanide Single-Molecule Magnets (SMMs) to "naked" gold nanoparticles we can explore the inherent magnetic properties of a hybrid magneto-plasmonic nanostructure using conventional magnetometry. Thus, through extensive study we have shown the potential for fundamental questions regarding surface attachment to be probed, while simultaneously exploring new applications of these unique systems.

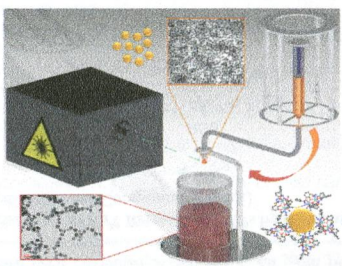

14419 dx.doi.org/10.1021/ic402710r

Diversity of Microstructural Phenomena in Superconducting and Non-superconducting $Rb_xFe_{2-y}Se_2$: A Transmission Electron Microscopy Study at the Atomic Scale

Maria V. Roslova, Oleg I. Lebedev, Igor V. Morozov, Saicharan Aswartham, Sabine Wurmehl, Bernd Büchner, and Andrei V. Shevelkov*

Iron vacancy ordering leads to a variety of superstructures in both superconducting and non-superconducting $Rb_xFe_{2-y}Se_2$ samples, whereas rubidium ordering (space group *Ammm* with the cell parameters $a = b = a_0\sqrt{2}$ and $c = c_0$) is observed in the superconducting sample only. A monoclinic distortion with $\beta \sim 87°$ accompanied by twinning discovered in the [110] zone-axis direction also appears to be a prerequisite of the superconducting $Rb_xFe_{2-y}Se_2$ material.

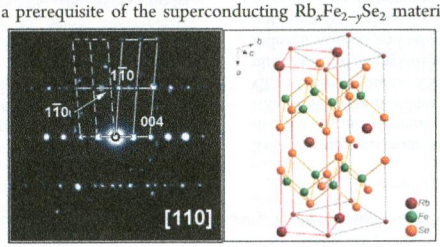

14428 S dx.doi.org/10.1021/ic402818g

Structural and Spectroscopic Investigation of an Anilinosalen Cobalt Complex with Relevance to Hydrogen Production
Amélie Kochem,* Fabrice Thomas, Olivier Jarjayes, Gisèle Gellon, Christian Philouze, Thomas Weyhermüller, Frank Neese, and Maurice van Gastel*

A Co(II) anilinosalen catalyst containing proton relays in the first coordination sphere has been spectroscopically and theoretically investigated. We show for the first time that the complex catalyzes the electrochemical production of hydrogen from acid in dichloromethane and acetonitrile solutions with a turnover frequency of 8 h^{-1}.

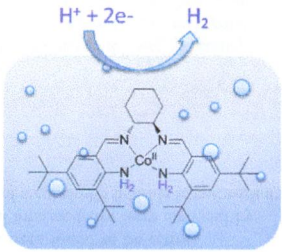

14439 S dx.doi.org/10.1021/ic402892f

From Sequential to One-Pot Synthesis of Dipyrrin Based Grid-Type Mixed Metal–Organic Frameworks
Antoine Béziau, Stéphane A. Baudron,* Audrey Fluck, and Mir Wais Hosseini*

The preparation of a series of grid-type mixed metal–organic frameworks (MM′MOFs) based on dipyrrin ligands appended with either a pyridyl or a phenyl-imidazolyl moiety can be performed by either a sequential or a one-pot synthetic strategy. The latter approach is efficient and more convenient than the earlier one, since the isolation, purification, and characterization of the, sometimes insoluble, metallatectons are not required.

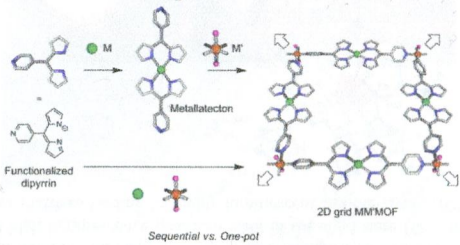

Additions and Corrections

14449 S dx.doi.org/10.1021/ic402856j

Correction to Elucidating Band-Selective Sensitization in Iron(II) Polypyridine-TiO_2 Assemblies
David N. Bowman, James H. Blew, Takashi Tsuchiya, and Elena Jakubikova*

S Supporting Information available via online article